

Recent results of the CMS experiment

Lars Sonnenschein^a

on behalf of the CMS collaboration

^a*III. Phys. Inst. A*

RWTH Aachen University

E-mail: Lars.Sonnenschein@cern.ch

The CMS experiment is a multi-purpose detector successfully operated at the LHC where predominantly pp collisions take place at various centre-of-mass energies up to $\sqrt{s} = 8$ TeV so far. Several weeks per year also heavy-ion collisions take place leading to interesting studies in Pb - Pb and p - Pb collisions at $\sqrt{s_{NN}} = 2.76$ TeV and $\sqrt{s_{NN}} = 5.02$ TeV centre-of-mass energies per nucleon, respectively. The excellent performance of the accelerator and the experiment allows for dedicated physics measurements over a wide range of subjects, starting from particle identification, encompassing forward physics, Standard Model measurements in multijet, boson, heavy flavour and top quark physics, building the basis for new physics searches interpreted within the framework of various models and theories. These pursued pp physics subjects are complemented by a rich heavy ion physics programme.

*52nd International Winter Meeting on Nuclear Physics,
January 27-31, 2014
Bormio Italy*

rounding the hadronic calorimeter. Its purpose is to bend the charged particle tracks, which in turn allows the determination of their momenta once the particle type is identified. Outside of the magnet are located four layers of gaseous muon chambers with excellent spatial resolution, complemented by resistive plate chambers with excellent temporal resolution, embedded between the iron return yoke to focus the magnetic flux inside the detector volume. The magnetic field at the muon detectors outside the solenoid amounts in average to about 2 T. Similar detector technologies are extended into the endcaps in form of disks for hermetic coverage.

The different subsystems of the CMS detector are operational to 98% in average (see Fig. 1, left), ranging from the highest data taking efficiency of nearly 100% reached by the hadronic calorimeter, to the lowest data taking efficiency of 96.3% of the silicon strips. Altogether there are about 80 million channels to be read out. During the Long Shutdown 1 (LS1) which is ongoing since February 2013 defect channels are being recovered. The high efficiency helps to keep the reconstruction and the comparison to simulation simple.

The rate of pp collisions produces a data volume corresponding to about 2 TB per second. To reduce this huge amount of data to a manageable size, a Level-1 trigger based on fast electronics implemented in programmable chips is employed. With an acceptance rate of up to 100 kHz the data is then sent to a computing farm at CMS with 2400 multicore Linux PC's, where the events are scrutinised with more sophisticated algorithms to make a final decision at this High Level Trigger [2] (HLT), if a given event might be of interest or can be discarded. The HLT accept rate can reach values closely above 2000 Hz. The rate of the most important triggers at HLT level agree with simulation within 5%. Over 300 TB local disk space permits the temporary storage of the data for up to one week. In normal operation the data is sent continuously to the CERN computing centre for storage, reconstruction and distribution to computing centres of participating institutions around the world. An overview of the CMS infrastructure and data flow is depicted in Fig. 1, right.

In 2011 (2012) up to 130 pb^{-1} (286 pb^{-1}) of integrated luminosity per day have been recorded [3][4]. Peak luminosities up to $40 \cdot 10^{32} \text{ Hz/cm}^2$ ($77 \cdot 10^{32} \text{ Hz/cm}^2$) have been reached in 2011 (2012) and integrated luminosities of 6.1 fb^{-1} (23.3 fb^{-1}) have been delivered by the LHC which had a proton run efficiency of 36.5% in 2012. The remainder of the time is dedicated to SetUp, Injection, Access, Squeeze and Ramp periods in decreasing order. The recorded data undergoes a certification process where depending on the operability of the various sub-detector systems and the needs for dedicated physics analyses two dataset categories are established. 85% of the data are certified as good where all sub-detectors have been fully operational. 90% of the data are certified as good for muon analyses disregarding calorimeter quality.

The number of parasitic pp collisions (referred to as pile-up events) accompanying a high energetic scattering of interest in a single LHC beam crossing is distributed according to a Poisson statistics with an average number of nine to ten events in 2011 and up to 25 events in 2012. In general the distinct vertices can be reconstructed to sort out interesting high energetic physics events from additional low energetic scattering background. The number of pile-up events increases with the number of instantaneous luminosity. A compromise is made between high luminosity and clean events for an optimised discovery potential.

In the last LHC run period (Run II) until LS1 proton proton collisions took place at a centre-of-mass energy of $\sqrt{s} = 8 \text{ TeV}$ with a proton bunch spacing of 50 ns. Data at previous centre-of-mass energies of $\sqrt{s} = 0.9, 2.76$ and 7 TeV with the same bunch spacing have been analysed

and are partly presented here. Dedicated run periods with heavy ion collisions at a centre-of-mass energy of 2.75 TeV (5.02 TeV) per nucleon in $Pb-Pb$ ($p-Pb$) collisions do also take place. One of the primary goals why the LHC has been built is the discovery of new physics, in particular the electro-weak symmetry breaking mechanism, also referred to as Brout-Englert-Higgs (BEH) mechanism which has been primarily conceived to endow the particles with mass. Experimental analysis of the Higgs boson particle predicted by this mechanism permits to probe the mathematical consistency of the Standard Model (SM) of particle physics beyond the TeV energy scale. The exploration of new energy frontiers at collider based experiments opens new possibilities on the way toward a unified theory. Potential discoveries could reveal the existence of supersymmetry, extra dimensions or dark matter at accessible energy scales. Parallel to the searches for new particles and new phenomena a rich programme of SM physics in various domains are conducted, including forward physics, multijet production, electro-weak vector boson production, heavy flavour physics, top quark physics. Furthermore heavy-ion collisions are exploited among others to study dense matter phases like quark-gluon plasma.

3. Forward and low x scale physics

At the LHC a wide range of proton momentum fractions x and momentum scales Q are accessible, extending the phase space of previous colliders considerably. In particular measurements at small x and scale are of interest for airshower experiments like Auger to improve the understanding and description of the interactions of cosmic rayons in the atmosphere. Small x at the LHC implies forward proton and diffractive physics while low scale implies soft physics in the underlying event. Several diffractive jet production mechanisms can be distinguished. In single diffractive pp collisions, where the two protons interact via one colourless double gluon exchange, also referred to as Pomeron, a rapidity gap separates the central hard scattering of the resolved proton and the proton which leaves the interaction intact into the forward direction. In double diffractive pp collisions

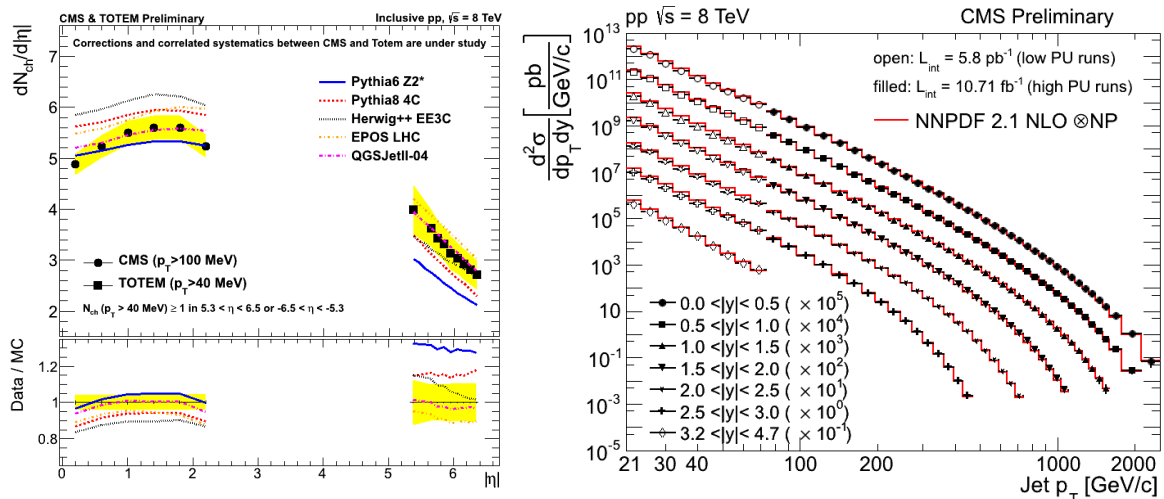


Figure 2: Left: Charged particle multiplicity distribution as a function of $|\eta|$. CMS covers the central pseudorapidities $|\eta| < 2.4$ and TOTEM the forward range $5.3 < |\eta| < 6.5$. Right: Inclusive jet cross section differentially in jet transverse momentum p_T and rapidity y . The low momentum region $21 < p_T < 74$ GeV is covered by low pile-up runs. The high momentum region $p_T > 74$ GeV is covered by high pile-up runs.

both protons which interact via a Pomeron get resolved and a rapidity gap is expected in the central region between the two hard jet activity regions. A further possibility provides the double Pomeron exchange, where both protons leave the collision intact into the forward direction but separated by two rapidity gaps a hard jet scattering takes place in the central rapidity region. In the following some forward and low x momentum fraction measurements are discussed.

The inelastic $p - Pb$ cross section at a nucleon nucleon centre-of-mass energy of $\sqrt{s_{NN}} = 5.02$ TeV has been measured [5]. Inelastic collisions are tagged using the hadronic forward calorimeters at pseudorapidities $3 < |\eta| < 5$. Two different event selections are used: A coincidence in both sides of the hadronic forward calorimeters and a single-sided event selection. These two selections have different sensitivity to contributions from photon induced (γp) collisions and hadronic diffractive interactions. The value of the hadronic inelastic cross section is measured within the CMS acceptance and extrapolated to its total value. The photon-induced contribution is subtracted. The final result $\sigma_{\text{inel.}} = 2.06 \pm 0.08$ b. The uncertainty is dominated by the determination of the luminosity. This measurement of the inelastic cross section is consistent with the expectation from the Glauber [6] approach ($\sigma_{\text{inel.}} = 2.13 \pm 0.04$ b), based on the pp cross section from the COMPETE [7] fit that has been extended by the TOTEM [8] measurement at a centre-of-mass energy of 7 TeV. Other model predictions are also compatible with the measurements given the experimental uncertainties. Only QGSJETII-04 predicts a value slightly above the upper uncertainty bound of this measurement.

Pseudorapidity and leading transverse momentum distributions of charged particles in pp collisions at $\sqrt{s} = 8$ TeV have been measured with the CMS and TOTEM detectors [9] in the pseudorapidity range of $|\eta| < 2.4$. The data correspond to an integrated luminosity of 17.4 nb^{-1} . Events are triggered by the TOTEM T2 telescopes covering the pseudorapidity range of $5.3 < |\eta| < 6.5$

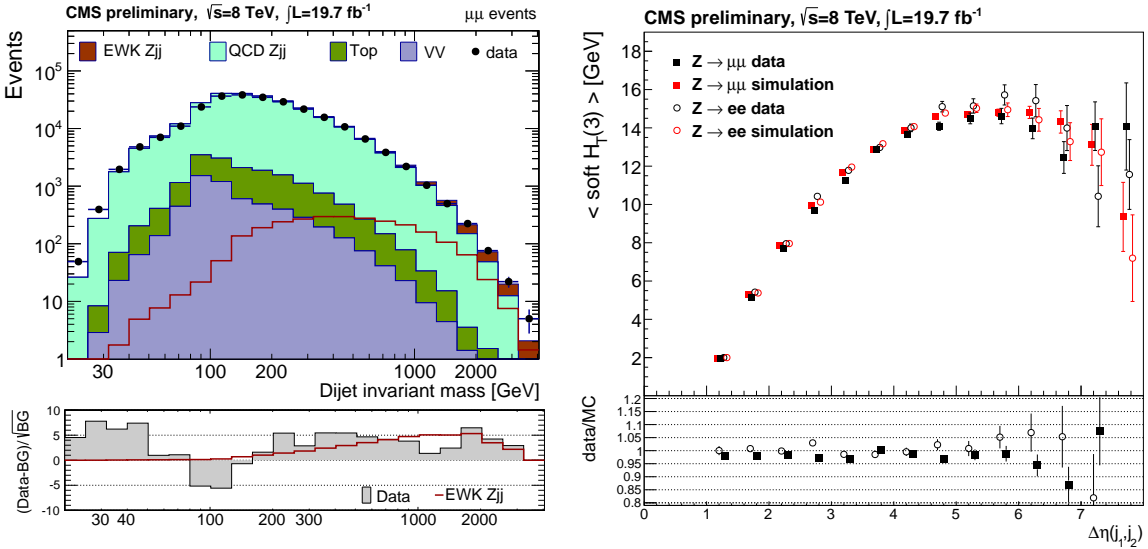


Figure 3: Dijet invariant mass distribution. The data is compared to different background contributions dominated by QCD production of Zjj and the signal (left). The scalar sum of the three leading transverse momentum track jets as a function of the pseudorapidity difference between the two tagged jets is shown in the right plot. The data is indicated in black, the simulation in red. The Drell-Yan (DY) dimuon channel is presented in squares, the dielectron channel in circles.

for reconstructed tracks above a transverse momentum threshold of 40 MeV. The measurement of the pseudorapidity distributions is performed for primary charged particles with $p_T > 0.1$ GeV and $p_T > 1$ GeV for two different selection criteria. An inclusive sample is obtained by requiring tracks reconstructed in the acceptance of the TOTEM T2 telescopes in either the forward or the backward hemispheres. The differential charged particle distribution as a function of $|\eta|$ is shown in Fig. 2 (left), covering the central CMS and forward TOTEM measurements, obtained by making use of low pile-up runs. Another sample enhanced in non-single diffractive dissociation events is obtained by requiring tracks in the T2 telescope in both forward and backward hemispheres. The average multiplicity per unit of pseudorapidity has been measured to be 5.4 ± 0.2 for the inclusive selection and 6.2 ± 0.3 for the Non Single Diffractive (NSD) enhanced sample, while for $p_T > 1$ GeV it has been measured to be 0.78 ± 0.03 and 0.93 ± 0.04 , respectively. At $\sqrt{s} = 8$ TeV, the average value of $dN_{ch}/d\eta|_{\eta=0}$ for the NSD-enhanced sample follows a power-like centre-of-mass energy dependence already suggested by previous NSD measurements at different energies. The measured charged-particle distributions can help to constrain the modelling of semi-hard (multi-)parton scattering processes in pp collisions at the LHC over large phase space regions in p_T and $|\eta|$. The transverse momentum distribution of the leading tracks in the central region is measured, too. The distribution integrated over the leading track transverse momentum above a $p_{T,\min}$ threshold shows a transition from a steeply falling distribution at large p_T (the perturbative region) to a flat distribution at small p_T (the non-perturbative region) for $p_{T,\min}$ of a few GeV. This region is not well described by current Monte Carlo event generators.

The inclusive jet cross section in proton-proton collisions at $\sqrt{s} = 8$ TeV has been measured [10] differentially in p_T for seven rapidity bins based on data collected with the CMS detector. The data set corresponds to an integrated luminosity of 5.8 pb^{-1} . The measurement was performed using the anti- k_T cluster jet algorithm with a distance parameter of $R = 0.7$ in the rapidity region of $|y| < 4.7$ for jet transverse momenta of $21 < p_T < 74$ GeV. The measured differential cross section is shown in Fig. 2 (right) in comparison to the NLO theory prediction. The open points cover this low momentum measurement. The dominant source of systematic uncertainty arises from the Jet Energy Scale (JES) which propagates about 5 - 45% uncertainty on the cross section measurement across varying rapidity bins. The measured jet cross-section is compared to predictions of next-to-leading order (NLO) QCD calculations taking non perturbative (NP) and Parton Shower (PS) forward folding into account. Within the current experimental and theoretical uncertainties, perturbative QCD calculations are in agreement with the measured inclusive jet cross sections.

The electro-weak production cross section of Z -bosons in the same flavour dilepton final state associated with two forward/backward jets in proton-proton collisions at $\sqrt{s} = 8$ TeV has been measured [11] based on a data sample recorded by the CMS experiment at the LHC with an integrated luminosity of 19.7 fb^{-1} . Different methods have been used to extract the signal, including a data-driven approach that models the QCD Zjj background based on γjj events. The cross section for this process is measured in dielectron and dimuon final states in the kinematic region with invariant masses of $m_{\ell\ell} > 50$ GeV, $m_{jj} > 120$ GeV, transverse momenta of $p_{Tj} > 25$ GeV and pseudorapidity $|\eta_j| < 5$. The dijet invariant mass distribution is given in Fig. 3, left and the distribution of the soft hadronic activity between the two jets is given at the right. Combining two different methods and channels, the cross section has been measured to $\sigma = 226 \pm 26(\text{stat}) \pm 35(\text{syst}) \text{ fb}$, in agreement

with the theoretical cross section at NLO which amounts to 239 fb. The hadronic activity in events with Z -boson production in association with jets is also studied, in particular in the rapidity interval between the two jets. The measured gap fractions for soft-hadronic vetoes show good agreement with different predictions.

4. Standard Model physics

The inclusive jet cross section, double-differential in jet transverse momentum p_T and absolute jet rapidity $|y|$, has been measured [12]. Data from LHC proton-proton collisions at $\sqrt{s} = 8$ TeV, corresponding to an integrated luminosity of 10.71 fb^{-1} have been collected with the CMS detector. Jets are reconstructed with the anti- k_T clustering jet algorithm with a distance parameter $R = 0.7$ in a phase space region covering jet transverse momenta between 74 GeV and 2.5 TeV and an absolute rapidity up to $|y| = 3.0$. The parton momentum fractions x probed in this measurement are given by the interval $0.019 < x < 0.625$. The measured differential cross section is shown in Fig. 2 (right) in comparison to the NLO theory prediction. The filled points cover this high momentum measurement, obtained by making use of high pile-up runs.

Dominant sources of experimental systematic uncertainties arise due to the jet energy scale (JES), unfolding and the luminosity measurement uncertainty. These lead to about 15-40% uncertainty in the cross section measurement across various rapidity bins. In comparison, the theory predictions are most affected by Parton Distribution Function (PDF) uncertainties, which amount to 10% to 50% depending on the rapidity bin, whereas choices of renormalisation and factorization scales contribute with 5% to 10% at central rapidity and with 40% in the outer rapidity bins. The measured jet cross section is corrected for detector effects and compared to predictions of perturbative QCD at NLO using various sets of PDF's. Some differences between the predictions employing various PDF sets and the data are observed, all of which are qualitatively covered by uncertainties in the low p_T region, except for the ABM11 PDF set, which exhibits significant deviations. In the high p_T region the CT10 theory prediction is in good agreement with data, whereas other PDF sets have significant differences compared to the measured cross section. This new inclusive jet cross section measurement probes a wide range in x and momentum scale Q . Therefore it can be exploited to constrain PDF's and to determine the strong coupling constant α_s in a new kinematic regime.

The inclusive jet cross section has been measured at $\sqrt{s} = 7$ TeV [13] extending the accessible phase space in jet transverse momenta up to 2 TeV. The absolute jet rapidities range up to 2.5. The experimental uncertainties of this measurement are smaller than in previous publications such that these data constrain the PDF's of the proton, notably for the gluon at high proton momentum fractions. Therefore this analysis provides valuable input to determine the strong coupling at high momentum scales. The impact on the extraction of the PDF's is investigated. The inclusion of CMS inclusive jet data in comparison to HERA inclusive DIS data alone significantly reduces the uncertainty on the gluon distribution for fractional parton momenta $x \gtrsim 0.01$. In particular model and parameterisation uncertainties of the up and down quark distributions decrease for x larger than 0.3. The effect is more pronounced for the up quark.

The jet data of this analysis has been included to fit the strong coupling constant as a free parameter in addition to the PDF's. This is not possible with HERA inclusive DIS data alone

showering scheme. Only moderate agreement between data and POWHEG [21] + PYTHIA Z2star for q_T below 20 GeV can be observed, whereas the description of PYTHIA with Z2star tune show better agreement. On the high q_T side of the spectrum better agreement of data with the predictions from the MADGRAPH [22] generator are observed. However, in the range of q_T beyond 100 GeV, the accuracy in data is not sufficient to significantly discriminate among available theoretical calculations of varying accuracy. In conclusion, the PYTHIA generator with Z2star tune is able to describe data well in the low q_T region, while MADGRAPH predictions are in general in good agreement with data at high q_T . The measurements done at 8 TeV are also compared with the ones at 7 TeV in terms of the ratio of the cross sections. An overall good agreement is observed in the ratio of data and the predictions from the theory.

A measurement of inclusive W and Z boson production cross sections in pp collisions at $\sqrt{s} = 8$ TeV is presented [23]. Electron and muon final states are analyzed in a data sample collected with the CMS detector corresponding to an integrated luminosity of $18.7 \pm 0.9 \text{ pb}^{-1}$. The W and Z bosons are observed via their decays into electrons and muons. Their measured inclusive cross sections are $\sigma(pp \rightarrow WX) \times Br(W \rightarrow \ell\nu) = 11.88 \pm 0.03(\text{stat}) \pm 0.22(\text{syst}) \pm 0.52(\text{lumi})$ nb and $\sigma(pp \rightarrow ZX) \times Br(Z \rightarrow \ell^+\ell^-) = 1.12 \pm 0.01(\text{stat}) \pm 0.02(\text{syst}) \pm 0.05(\text{lumi})$ nb limited to a dilepton mass range of 60 to 120 GeV. Ratios of cross sections are also produced. The measurements are consistent between the electron and muon channels, and in agreement with Next-to-Next-to-Leading Order (NNLO) QCD cross-section calculations.

A study of the $WV\gamma$ three electro-weak boson production and the anomalous quartic gauge boson couplings have been measured [24], based on events containing a W boson decaying to leptons, a second vector boson V (W or Z boson) decaying to two jets, and a photon.

Together with the triple $WW\gamma$ and WWZ gauge boson vertices, the SM predicts the existence of quartic $WWWW$, $WWZZ$, $WWZ\gamma$ and $WW\gamma\gamma$ vertices. The direct investigation of gauge boson self-interactions provides a crucial test on the gauge structure of the SM and is expected to play a significant role at LHC energies. The data analyzed corresponds to 19.3 fb^{-1} of integrated luminosity from pp collisions at $\sqrt{s} = 8$ TeV collected in 2012 by the CMS detector at the Large Hadron Collider. For this amount of data an upper limit of 241 fb is set at 95% confidence level for $WV\gamma$ production with photon $p_T > 10$ GeV. No evidence of anomalous $WW\gamma\gamma$ and $WWZ\gamma$ quartic gauge couplings is found. The following 95% confidence level upper limits are obtained for these couplings: $-21 < a_0^W/\Lambda^2 < 20 \text{ TeV}^{-2}$, $-34 < a_C^W/\Lambda^2 < 32 \text{ TeV}^{-2}$, $-25 < f_{T,0}/\Lambda^4 < 24 \text{ TeV}^{-4}$, $-12 < \kappa_0^W/\Lambda^2 < 10 \text{ TeV}^{-2}$ and $-18 < \kappa_C^W/\Lambda^2 < 17 \text{ TeV}^{-2}$. A comparison to previous measurements of the LEP experiment L3 for the vertex $WW\gamma$ and of the DØ experiment for the vertex $\gamma\gamma \rightarrow WW$ is given in Fig. 4 (right). This is the first time ever that limits on $f_{T,0}$ and the CP conserving couplings κ_0^W and κ_C^W are reported.

5. Heavy flavour physics

Dedicated low p_T threshold dimuon triggers with a narrow mass window around resonances such as J/ψ , ψ' , B_s and Υ have been exploited in low luminosity periods with relatively low number of pile-up events per proton bunch crossing. The invariant dimuon mass spectrum for the different applied dimuon triggers is shown in Fig. 5 (left). Of particular interest here is the measurement of the Branching Fraction (BF) of the decay $B_s \rightarrow \mu^+\mu^-$ which is highly suppressed in the SM and

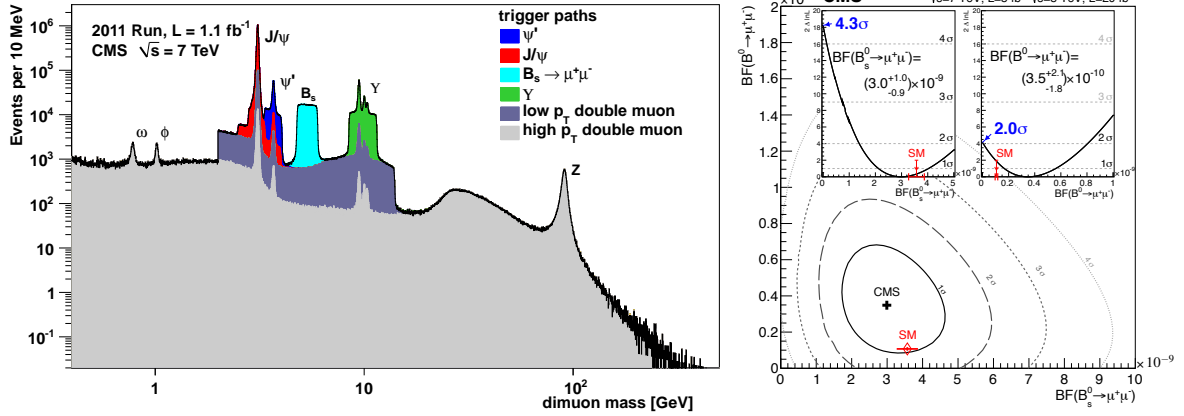


Figure 5: Left: Dimuon invariant mass spectrum. Shown are dedicated low p_T threshold dimuon triggers with a narrow mass window around resonances like B_s . Right: CMS obtained values for the branching fractions of $B_d \rightarrow \mu^+\mu^-$ and $B_s \rightarrow \mu^+\mu^-$. The insets show the likelihoods of the one-dimensional projections with the corresponding significances. The SM expectation value is indicated in red.

new particles could contribute in loop and box diagrams and enhance the BF. Within the Minimal Supersymmetric SM (MSSM) the BF is proportional to the sixth power of the ratio $\tan\beta$ of the two Higgs doublets vacuum expectation values. The likelihood for the BF's obtained by CMS for the two processes $B_d \rightarrow \mu^+\mu^-$ and $B_s \rightarrow \mu^+\mu^-$ exploiting the full integrated luminosity of 5 fb^{-1} at $\sqrt{s} = 7 \text{ TeV}$ and 20 fb^{-1} at $\sqrt{s} = 8$ in pp collisions are shown in Fig. 5 (right) in agreement with the SM expectation. The numerical results are $BF(B_s^0 \rightarrow \mu^+\mu^-) = 2.9^{+1.1}_{-1.0}(\text{stat})^{+0.3}_{-0.1}(\text{syst}) \times 10^{-9}$, corresponding to a 4.0 standard deviations evidence and $BF(B_d^0 \rightarrow \mu^+\mu^-) = 3.5^{+2.1}_{-1.8} \times 10^{-10}$, corresponding to a 2.0 standard deviations significance. In assuming a Null hypothesis the later BF measurement can also be expressed in terms of a limit, namely $BF(B_d^0 \rightarrow \mu^+\mu^-) < 7.4 \times 10^{-10}$ at 95% Confidence Level (C.L.). In combination with the LHCb results exploiting an integrated luminosity of 3 fb^{-1} , the decay $B_s \rightarrow \mu^+\mu^-$ has been observed with a Branching Fraction of $BF(B_s^0 \rightarrow \mu^+\mu^-) = (2.9 \pm 0.7) \times 10^{-9}$ in consistency with the SM expectation and the combination for the decay $B_d \rightarrow \mu^+\mu^-$ yields $BF(B_d^0 \rightarrow \mu^+\mu^-) = 3.6^{+1.6}_{-1.4} \times 10^{-10}$ which is not yet statistically significant but again consistent with the SM expectation.

6. Top quark physics

The top quark is the heaviest known particle to-date and it is produced pair-wise or singly with associated particles. The $t\bar{t}$ production at the LHC in pp collisions is dominated by gluon gluon fusion (90%), the remainder being due to quark antiquark annihilation (10%). At a centre-of-mass energy of $\sqrt{s} = 7 \text{ TeV}$ the NLO cross section [25] yields 158 pb and the approximated NNLO cross section [26] 163 pb. At $\sqrt{s} = 8 \text{ TeV}$ the approximated NNLO cross section amounts to 246 pb. In the SM the top quark decays almost exclusively into a W boson and a b quark. The W boson in turn decays in 2/3 of cases into a $q\bar{q}$ pair and in 1/3 of cases leptonically. Single top quark production is dominated by the t -channel with a cross section of 64 pb at $\sqrt{s} = 7 \text{ TeV}$ and 87 pb at $\sqrt{s} = 8 \text{ TeV}$, followed by the tW -channel with 15.7 pb (22.4 pb) at $\sqrt{s} = 7(8) \text{ TeV}$ and the s -channel with 4.6 pb (5.6 pb) at $\sqrt{s} = 7(8) \text{ TeV}$.

The $t\bar{t}$ cross section measurements are done in all possible decay channels by means of a binned likelihood fit at $\sqrt{s} = 7$ and 8 TeV. The $e/\mu + \text{jets}$ channel [27] yields a cross section of $\sigma(t\bar{t}) = 228 \pm 9(\text{stat})_{-26}^{+29}(\text{syst}) \pm 10(\text{lumi})$ pb, the $ee, e\mu, \mu\mu$ channel [28] yields $\sigma(t\bar{t}) = 227 \pm 3(\text{stat}) \pm 11(\text{syst}) \pm 10(\text{lumi})$ pb which at the same time corresponds to the numbers of the combination of the two channels due to the larger errors of the former one and the agreement between the channels which amounts to the 5 - 15% level of experimental uncertainty. The measurements are compatible with the theory prediction in approximated NNLO with scale and PDF uncertainties of the order 10%. A full NNLO prediction is available and reduces this uncertainty to about 4%. Therefore the cross section measurements can be exploited to probe the gluon density of the proton. Single top quark production has been measured in the t -channel with the W boson decaying leptonically at $\sqrt{s} = 7$ [31] yielding $\sigma = 70.2 \pm 5.2(\text{stat}) \pm 10.4(\text{syst}) \pm 3.4(\text{lumi})$ pb and at $\sqrt{s} = 8$ TeV [32] yielding $\sigma = 80.1 \pm 5.7(\text{stat}) \pm 11.0(\text{syst}) \pm 4.0(\text{lumi})$ pb. The t -channel single top production is also being exploited for a direct measurement of the CKM matrix element $|V_{tb}| = \sqrt{\sigma_t/\sigma_t^{\text{theo}}(|V_{tb}| \equiv 1)} = 1.04 \pm 0.09(\text{exp}) \pm 0.02(\text{theo})$. In the tW -channel the cross section has been observed [34] at $\sqrt{s} = 8$ TeV to be $\sigma = 23.4_{-5.4}^{+5.5}$ pb with a significance of 6.0σ and in agreement with the SM prediction. At $\sqrt{s} = 7$ TeV a 4.0 standard deviations evidence [33] for tW production has been obtained with a cross section of $\sigma = 16_{-4}^{+5}$ pb in agreement with the SM prediction. The 2012 dataset at $\sqrt{s} = 8$ TeV with an integrated luminosity of 19.3 fb^{-1} leads to an upper limit on the s -channel cross section times branching ratio of 11.5 pb at 95% C. L. [35]. Figure 6, left shows the single top cross section measurements of the different channels and centre-of-mass energies in comparison to the SM predictions. The right plot of Fig. 6 shows the top mass measurements in the different decay channels from CMS and ATLAS in comparison to theory. The dilepton channel is treated as a counting experiment. The hadronic channel making use of an unbinned likelihood is taken as one bin. The Best Linear Unbiased Estimate (BLUE) method [36] is used as a cross check for the combination of the different channels taking into account correlations between different contributions to the measurements. The top mass combination of CMS and ATLAS for the 2011 dataset at $\sqrt{s} = 7$ TeV yields $m_{\text{top}} = 173.29 \pm 0.23(\text{stat}) \pm 0.26(\text{iJES}) \pm 0.88(\text{syst})$ GeV [37] where iJES indicates the error due to intercalibration Jet Energy Resolution due to modelling of ra-

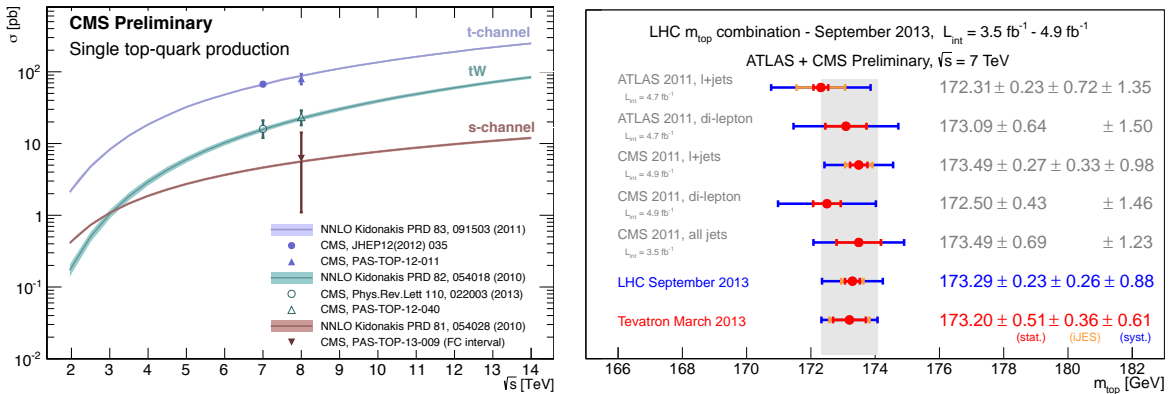


Figure 6: Left: Measured cross sections of single top production for the different production channels at $\sqrt{s} = 7$ and 8 TeV in comparison to the NNLO predictions. Right: LHC top mass combination in comparison to the Tevatron combination.

diation in the jet differences in η and p_T . This result is competitive with the Tevatron combination $m_{\text{top}} = 173.20 \pm 0.51(\text{stat}) \pm 0.36(\text{iJES}) \pm 0.61(\text{syst})$ GeV. The systematic error is below 1 GeV and the statistical and iJES uncertainties are smaller than the Tevatron combination.

7. Standard Model Higgs boson physics

The electro-weak symmetry breaking mechanism, also referred to as Brout-Englert-Higgs (BEH) mechanism has been primarily conceived to endow the particles with mass. Experimental analysis of this mechanism will allow to probe the mathematical consistency of the Standard Model (SM) of particle physics beyond the TeV energy scale where divergences of the theoretical description can be prevented by means of loop corrections taking contributions and couplings to a scalar Higgs boson into account. Several production mechanisms contribute at the LHC, namely the dominant gluon fusion process, the subdominant vector boson fusion and the associated production process. The associated production via a vector boson suffers a high level of multijet background and is less favoured compared to the Tevatron where the reach is limited to relatively low Higgs boson masses [38]. The associated production in $t\bar{t}$ events is too small for reach within the existing datasets. Present CMS exclusion limits for $t\bar{t}H$ production with $H \rightarrow \gamma\gamma$ are about five times above the SM expectation [39].

The Higgs boson Yukawa coupling strength is proportional to the mass of the particles, favouring the coupling via a top quark loop. Photons and gluons can only couple indirectly. The decay modes and branching ratios depend on the Higgs boson mass. At the mass of 126 GeV $H \rightarrow b\bar{b}$ is the dominant decay channel, followed by the decays into WW , gg , $\tau\tau$, $c\bar{c}$, ZZ , $\gamma\gamma$ and $Z\gamma$. Most decay modes are pursued by CMS. Table 1 shows for the most important Higgs decay channels analysed by CMS the signal signatures, the Signal over Background (S/B) ratio, the mass resolution at $m_H = 126$ GeV, the number of events with an integrated luminosity of 20 fb^{-1} and Higgs boson properties which can be probed.

The CMS data has been analysed to study a standard model Higgs boson in the four-lepton decay channel $H \rightarrow ZZ \rightarrow 4\ell$ ($\ell = e, \mu$) and $H \rightarrow ZZ \rightarrow 2\ell\tau$ [40]. The mass distributions are

Decay channel	Signature	S/B	Mass resolution @ 126 GeV	N events in 20 fb^{-1}	Probing
$H \rightarrow b\bar{b}$	two b jets, Z or W , $b\bar{b}$ inv. mass	low $\mathcal{O}(0.1)$	10%	$\sim 10^5$ 50 selected	couplings to fermions
$H \rightarrow \tau\tau$	had. τ , ℓ 's, MET	low $\mathcal{O}(0.1)$	15%	$\sim 10^4$ 40 selected	couplings to fermions
$H \rightarrow WW$	$\ell^\pm\ell^\mp$ pair, MET	medium $\mathcal{O}(1)$	—	$\sim 10^3$ 120 selected	σ , BR , couplings to V H mass,
$H \rightarrow \gamma\gamma$	two γ 's, inv. mass peak	low $\mathcal{O}(0.1)$	2%	~ 800 400 selected	κ_V , κ_F couplings, discovery
$H \rightarrow ZZ$	four ℓ 's, with Z and H mass peaks	high $> \mathcal{O}(1)$	1 - 2%	~ 40 12 selected	H mass, discovery

Table 1: Characteristics of the most important Higgs channels analysed by the CMS experiment.

measured with four-lepton invariant masses above a threshold of 100 GeV exploiting 5.1 fb^{-1} of integrated luminosity at $\sqrt{s} = 7 \text{ TeV}$ and 19.6 fb^{-1} at $\sqrt{s} = 8 \text{ TeV}$. To discriminate background, information on an event-by-event basis is used from the measured four-lepton mass, the mass uncertainty, a kinematic discriminant and information sensitive to the production mechanism, such as associated dijet characteristics and transverse momentum of the four-lepton system. Upper limits at 95% C.L. exclude the SM-like Higgs boson in the range of 130 – 827 GeV while the expected exclusion range amounts to 113.5 – 778 GeV. The new boson discovered by the CMS and ATLAS experiments is observed in the 4 lepton channel measured by CMS, with a local significance of 6.7 standard deviations above the expected background. Figure 7 (left) shows the invariant four lepton mass distribution of signal compared to the expected SM background. A measurement of its mass yields $125.8 \pm 0.5(\text{stat}) \pm 0.2(\text{syst}) \text{ GeV}$. The signal strength μ relative to the expectation for a standard model Higgs boson, is measured to be $\mu = 0.91^{+0.30}_{-0.24}$ at the mass where the boson has been found. The signal strength modifiers associated with vector bosons and fermions in the production mechanism are measured to be $\mu_V = 1.0^{+2.4}_{-2.3}$ and $\mu_F = 0.9^{+0.5}_{-0.4}$ in consistence with the SM expectations. The spin-parity of the boson is studied and the pure scalar hypothesis is found to be consistent with the observation. The measured state has been compared to six other spin-parity hypotheses including spin 0, 1 and 2 states with positive and negative spin-parity. Figure 7 (right) shows the comparison of the scalar and pseudoscalar Higgs boson hypotheses. The CMS measurement is indicated by the red arrow and clearly disfavour a pseudoscalar Higgs boson. The fraction of a CP-violating contribution to the decay amplitude, expressed through the fraction f_{a3} of the corresponding decay rate, is measured to be $f_{a3} = 0.00^{+0.23}_{-0.00}$ again consistent with the SM expectation. The data disfavour the pure pseudoscalar hypothesis 0 with a CL_s value of 0.16%. This disfavour the pure spin-2 hypothesis of a narrow resonance with minimal couplings to the vector bosons with a CL_s value of 1.5%. The spin-1 hypotheses are disfavoured with an even higher level of confidence.

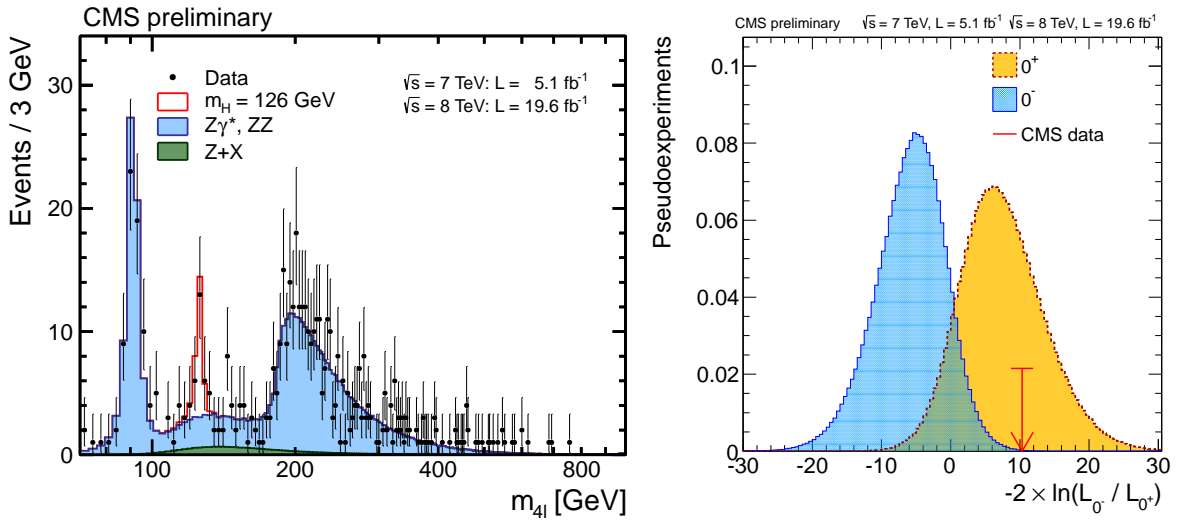


Figure 7: Left: Invariant mass distribution of the four leptons indicating clearly the peak at $m_H = 125.8 \text{ GeV}$, exploiting the statistics of the full 2011 (5.1 fb^{-1} at $\sqrt{s} = 7 \text{ TeV}$) and 2012 (19.6 fb^{-1} at $\sqrt{s} = 8 \text{ TeV}$) datasets. Right: Measurement of the spin-parity of the found Higgs boson, strongly favouring a scalar Higgs boson and disfavouring a pseudoscalar Higgs boson.

Evidence for the standard model Higgs boson decaying into a pair of τ leptons has been established [41]. The analysis is based on the full pp collision data sample recorded by CMS in 2011 and 2012, corresponding to an integrated luminosity of 4.9 fb^{-1} at a $\sqrt{s} = 7 \text{ TeV}$ and 19.4 fb^{-1} at $\sqrt{s} = 8 \text{ TeV}$. It is performed in five different final states, $\mu\tau_h$, $e\tau_h$, $e\mu$, $\tau_h\tau_h$ and $\mu\mu$. These channels are combined with the result of a search for the standard model Higgs boson decaying into a pair of τ leptons where the Higgs boson is produced in association with W or Z bosons decaying leptonically. An excess of events is observed over the expected background contributions, with a maximum local significance of 3.2 standard deviations for m_H values between 115 and 130 GeV. The best fit of the observed $H \rightarrow \tau\tau$ signal cross section for $m_H = 125 \text{ GeV}$ is 0.78 ± 0.27 times the SM expectation. These observations constitute evidence for the 125 GeV Higgs boson decaying to a pair of τ leptons.

The Higgs signal strengths $\mu = \sigma/\sigma_{SM}$ have been measured in many decay channels and associated production modes. The combination of the best fit values amounts to $\mu = 0.80 \pm 0.14$ for a Higgs boson mass of $m_H = 125.7 \text{ GeV}$. The couplings strengths to fermions κ_F and to bosons κ_V have also been measured and the combination of various analysis channels are close to the SM expectation. Systematic and theoretical uncertainties arising e.g. from QCD scale, PDF's and Br 's are taken into account.

Projections of Higgs boson measurements with 300 fb^{-1} at $\sqrt{s} = 14 \text{ TeV}$ [42] have been studied. The performance estimation is based on extrapolation of ICHEP 2012 performance. There is potential to shrink the errors by a factor 2 - 4 on SM Higgs boson signal and coupling strengths.

8. Search for supersymmetry

In the supersymmetric extension of the Standard Model corresponds to each SM particle a supersymmetric partner particle with identical gauge quantum numbers but spin differing by 1/2. The primary motivation to introduce SUPerSYmmetry (SUSY) is to solve the hierarchy problem. Large fine-tuning is needed for physical parameters of a theory at high energy scale in order to correctly describe the low-energy scale and light objects. To keep the renormalised Higgs boson mass at the weak scale the bare mass requires an unnatural fine-tuning of the order $(M_W/M_{GUT})^2 \sim 10^{-28}$. Quadratic divergences due to loop corrections can be canceled by adding supersymmetric partner particles. The highest expected production cross sections of supersymmetric particles at the LHC are given by gluino and squark pair production, followed by the electro-weak production of charginos and neutralinos. The decay topology and kinematics is characterised by high transverse momentum jets, \cancel{E}_T due to the undetected Lightest Supersymmetric Particle (LSP) and neutralino and chargino decays into SM fermion pairs and the LSP which serves as a dark matter candidate in the case of R -parity conservation, where R -parity is defined as $R_p = (-1)^{3(B-L)+2s}$ with $B = \text{Baryon number}$, $L = \text{Lepton number}$ and $s = \text{spin}$. For supersymmetric particles holds $R_p = -1$ and for SM particles $R_p = +1$.

In section 5 the observation of $B_S \rightarrow \mu\mu$ and its implications for new physics, in particular for SUSY has been discussed. The measurement of the branching ratio $Br(B_S \rightarrow \mu\mu)$ is consistent with the SM expectation which causes severe constraints on new physics. In particular for the Constrained Minimal Supersymmetric SM (CMSSM) direct and indirect constraints suggest particle masses at the multi-TeV level. This implies that sparticle masses are mostly out of reach for

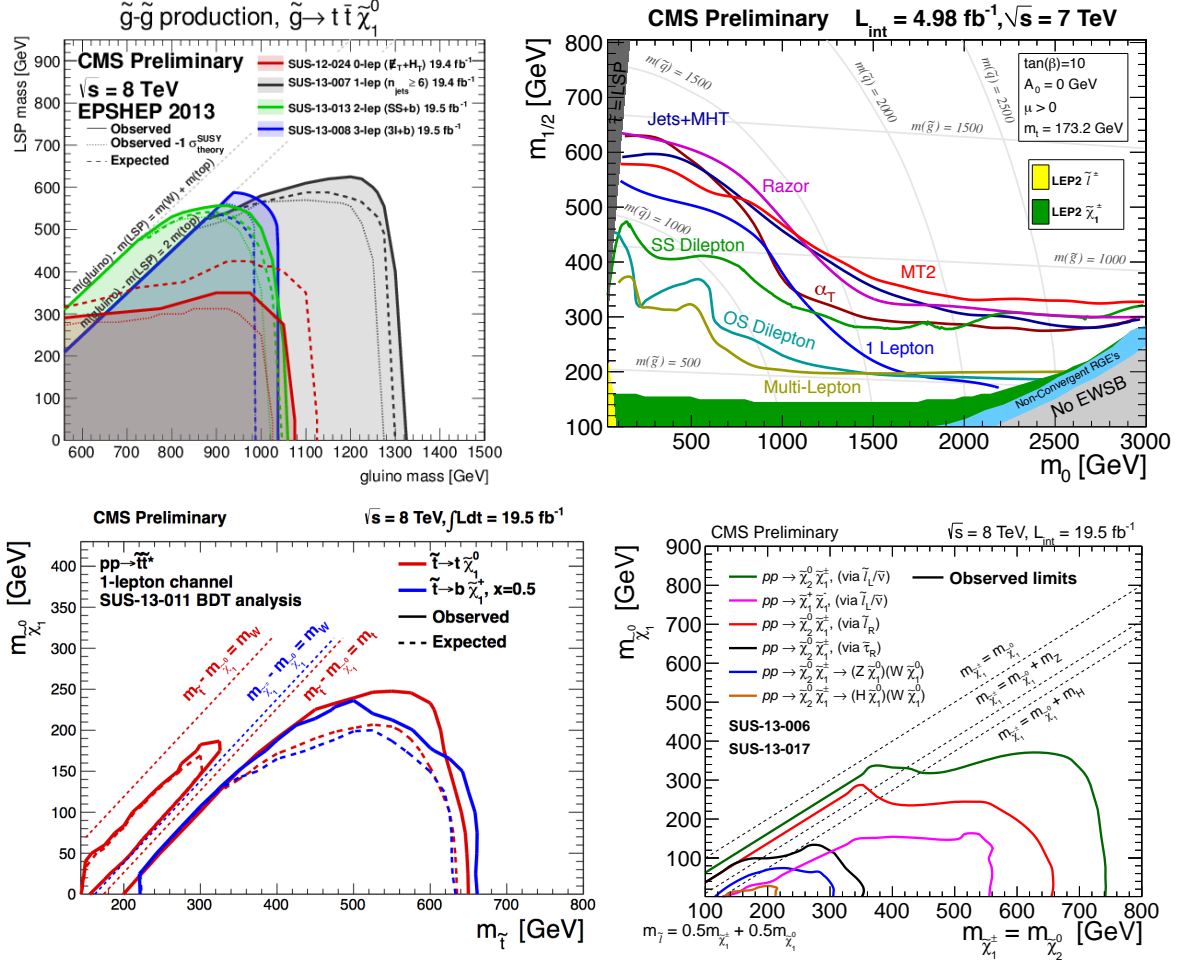


Figure 8: SUSY exclusion summaries. Top left: Limits on gluino pair production ($\tilde{g} \rightarrow t\bar{t}\tilde{\chi}_1^0$). Top right: CMSSM mSUGRA limits in the plane of gaugino mass $m_{1/2}$ vs. scalar mass m_0 for $\tan\beta = 10$, $A_0 = 0$ GeV, $\mu > 0$ of various analyses on the 2011 dataset with $\sqrt{s} = 7$ TeV. Bottom left: Limits on direct stop production. Bottom right: Limits on electro-weak gaugino production.

the LHC. More severe, fine-tuning will be required for the CMSSM. Models beyond the CMSSM provide viable options. Notably third generation sfermions might be in reach. First and second generation sfermions can be made much heavier naturally. Also the electro-weak SUSY sector might be in reach (light higgsino). Considerable phase space is accessible at the LHC.

A natural SUSY scenario with gauge-mediated SUSY breaking (GMSB) has been searched for [43] in the context of simplified model sparticle mass spectra (SMS), where the potential signal is given by Feynman graphs describing the production mechanism and the decay chains. The sparticle masses are free parameters of such SMS. The natural GMSB higgsino model chosen assumes that only the stop and the higgsino are accessible. The other sparticles are assumed to be located at higher mass scales out of reach for the LHC. In the strong production a pair of stop quarks is produced with b quarks in the decay and Higgs bosons as well as the gravitino as LSP in the final state. The branching ratio of the lightest neutralino into Higgs and gravitino is assumed to be one: $Br(\tilde{\chi}_1^0 \rightarrow H\tilde{G}) = 1$. In the electro-weak production a pair of gauginos (charginos or neutralinos) is produced, again with Higgs bosons and gravitino LSP's in the final state. Events are

selected in which there are two photons comprising a Higgs boson candidate, at least two b -jets and missing transverse energy (E_T^{miss}). Exploiting an integrated luminosity of 19.5 fb^{-1} in pp collisions at $\sqrt{s} = 8 \text{ TeV}$ no evidence of a signal has been found and lower limits at the 95% C.L. on the stop mass between 360 to 410 GeV have been set, depending on the higgsino mass.

Searches for direct gluino pair production are accomplished in the 0-lepton channel [45] based on missing transverse energy E_T^{miss} and transverse hadronic scalar momentum H_T , in the 1-lepton channel [46] based on at least six jets in the hadronic final state, in the 2-lepton channel [47] based on Same Sign (SS) leptons and b -tagged jets and in the 3-lepton channel [48] based on three leptons and b tagged jets. Limits are derived in the kinematic phase space of LSP mass vs. gluino mass $m_{\tilde{g}}$, excluding gluino masses up to 1350 GeV.

Due to the strong constraints on the CMSSM from direct LHC searches and the Higgs boson found at a mass of about 126 GeV it will not be able to solve the hierarchy problem anymore. Therefore CMS does no longer provide CMSSM interpretations for searches accomplished from the $\sqrt{s} = 8 \text{ TeV}$ 2012 dataset on. Therefore the last CMS CMSSM mSUGRA limit interpretations have been applied to the $\sqrt{s} = 7 \text{ TeV}$ 2011 dataset. The limits in the gaugino mass $m_{1/2}$ vs. scalar mass m_0 plane for $\tan\beta = 10$, $A_0 = 0 \text{ GeV}$, $\mu > 0$ are summarized in Fig. 8, top right plot for various analyses with different production mechanisms and final states.

A search for the direct pair production of top squarks, in the final state consisting of a single isolated lepton, jets, large missing transverse energy and large transverse mass has been performed. Signal regions are defined by means of the output of a Boosted Decision Tree (BDT) multivariate discriminator and requirements on several kinematic discriminants. Two kinematic signal regions between the boundary conditions $m_{\tilde{t}} - m_{\tilde{\chi}_1^0} = m_W$ and $m_{\tilde{\chi}_1^\pm} - m_{\tilde{\chi}_1^0} = m_W$ on the one hand and beyond $m_{\tilde{t}} - m_{\tilde{\chi}_1^0} = m_t$ on the other hand are considered as can be seen in Fig. 8, top left plot. The observed yields in the signal regions agree with the predicted backgrounds within uncertainties. The results are interpreted in the context of models of top-squark pair production and decay, probing top squarks with masses up to about 650 GeV.

Searches for the electro-weak production of gauginos (neutralinos $\tilde{\chi}^0$ and charginos $\tilde{\chi}^\pm$) are accomplished with sleptons in the decay chain [49] giving rise to leptons and E_T^{miss} in the final state. Another analysis is looking for a W and a Higgs boson in the decay chain [50], the W boson decaying leptonically and the Higgs boson giving rise to two b -jets. LSP $\tilde{\chi}_1^0$ masses are excluded up to 350 GeV and chargino masses $\tilde{\chi}_1^\pm$ up to 740 GeV. All approved CMS SUSY results and summaries are publically available at

<https://twiki.cern.ch/twiki/bin/view/CMSPublic/PhysicsResultsSUS>.

9. Exotic searches for new physics

Many searches for new physics are pursued by the CMS experiment, ranging from compositeness, over heavy resonances, long lived particles, lepto-quarks, fourth generation particles and contact interactions to extra dimensions and black holes. Limits and their summaries on particle masses and effective energy scales at which new physics sets in can be found at

<https://twiki.cern.ch/twiki/bin/view/CMSPublic/PhysicsResultsEXO>.

Here a dark matter analysis [51] will be detailed as an example of the rich search for new physics programme conducted by the CMS experiment.

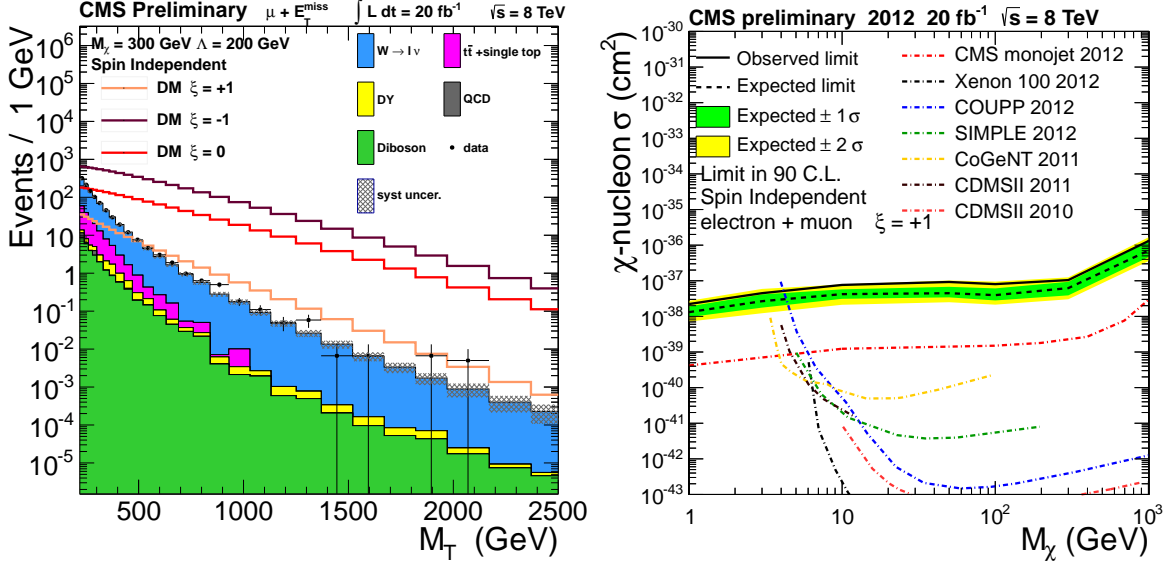


Figure 9: Left: Distribution of the transverse mass determined from the lepton and E_T^{miss} for the data in good agreement with the SM background predictions. Possible Dark Matter (DM) signals with different interference coefficients ξ are superposed. Right: Limits interpretation of the DM-nucleon cross section as a function of the DM particle mass M_χ . Limits of dedicated astrophysics experiments and the CMS monojet analysis are also given.

A search for new physics in final states with an electron or a muon and E_T^{miss} due to particles escaping the detector undetected has been performed. The results can be interpreted in terms of the cross section of events with a W boson recoiling against a pair of Dark Matter (DM) particles in an effective theory. Such a process would reveal in the detector as a lepton plus E_T^{miss} in the final state. The reconstructed transverse mass distribution of the CMS data in good agreement to SM backgrounds is shown in Fig. 9 (left). The DM model considers two possible couplings, vector- and axial-vector like. They could couple to up- and down-type quarks with different strengths, parameterised by a coefficient ξ . Possible consequences on the signal cross section and shape are investigated. The results are presented in terms of production cross section limits, which are transformed to limits on the effective parameter Λ and M_χ -proton cross sections as measured directly by dedicated astrophysics experiments. Figure 9 (right) shows the limits on the χ -nucleon cross section as a function of the DM mass M_χ . The limits derived on Λ are $\Lambda < 1000/700/300$ GeV for $\xi = -1/0/+1$, for both vector and axial-vector couplings.

10. Heavy ion physics

Studies of multi-particle correlations play a major role in the characterisation of the underlying mechanism of particle production in high energy collisions of protons with nuclei. Of particular interest in relativistic nucleus-nucleus (AA) collisions is the observed long-range (large $|\Delta\eta|$) structure in two-dimensional (2D) $\Delta\eta - \Delta\phi$ correlation functions. A source of such long-range correlations is the elliptic flow, induced by the hydrodynamic evolution of the collision zone in non-central nucleus-nucleus interactions. A dedicated high-multiplicity trigger was implemented making use of at least one charged particle track with $p_T > 0.4$ GeV in the pixel tracker. The observed long-

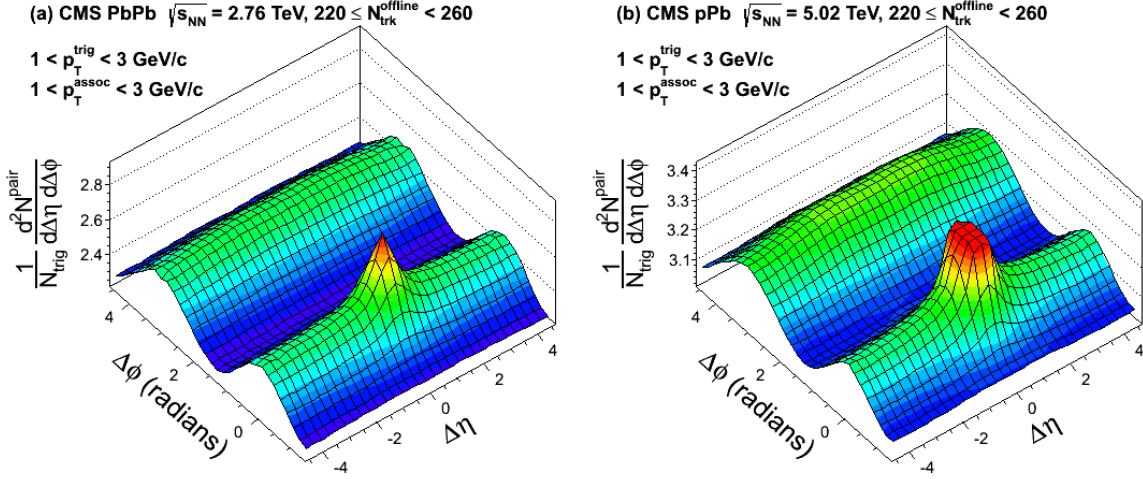


Figure 10: 2D two-particle correlation functions for 2.76 TeV $Pb - Pb$ (left) and 5.02 TeV $p - Pb$ (right) collisions for pairs of charged particles with $1 < p_T^{\text{trig}} < 3$ GeV and $1 < p_T^{\text{assoc.}} < 3$ GeV within the $220 \leq N_{\text{trk}}^{\text{offline}} < 260$ multiplicity bin. The sharp near-side peak from jet correlations is truncated to emphasize the structure outside that region.

range correlations can be attributed to the collective expansion of a strongly-interacting medium. In $p - Pb$ collisions, the overall strength of the near-side correlation is found to be significantly greater than in pp collisions. The two-particle correlations are shown in Fig. 10 for $Pb - Pb$ (left) and $p - Pb$ collisions for pairs of charged particles with $1 < p_T^{\text{trig}} < 3$ GeV and $1 < p_T^{\text{assoc.}} < 3$ GeV within the $220 \leq N_{\text{trk}}^{\text{offline}} < 260$ track multiplicity range. For $Pb - Pb$ collisions, this $N_{\text{trk}}^{\text{offline}}$ range corresponds to an average centrality of approximately 60%. In addition to the correlation peak near $(\Delta\eta, \Delta\phi) = (0, 0)$ due to jet fragmentation a pronounced long-range structure is seen at $\Delta\phi \simeq 0$ extending at least 4.8 units in $|\Delta\eta|$. On the away side ($\Delta\phi \simeq \pi$) of the correlation functions, a long-range structure is also seen and found to exhibit a magnitude similar to that on the near side for this p_T range. In non-central AA collisions this $\cos(2\Delta\phi)$ -like azimuthal correlation structure is assumed to arise primarily from elliptic flow. The away-side correlations must also contain contributions from back-to-back jets, which need to be accounted for, before extracting any other source of correlations.

Conclusions

The LHC accelerator and the CMS experiment provide an excellent performance. Maintenance, upgrades and optimisations in the present Long Shutdown 1 (LS1) phase are on track. Forward physics has been accomplished at the LHC at small proton momentum fractions and forward rapidities unprecedented at previous colliders. The Standard Model (SM) has been confirmed, precision measurements have been refined. A Higgs-like boson has been found and properties are consistent with the assumption of a SM Higgs boson. The highest collider energy frontier is being explored. The decay $B_s \rightarrow \mu\mu$ has been observed (CMS + LHCb combination). Its Branching ratio is consistent with the SM expectation, putting severe constraints on new physics, in particular rendering the Constrained Minimal Supersymmetric SM (CMSSM) unnatural, i.e. requiring fine-tuning. The search for evidence of new physics has been accomplished in many channels.

Long-range correlations in proton-nucleon and nucleon-nucleon collisions provide important studies on the way for an understanding of the quark-gluon plasma. More LHC data will be taken at $\sqrt{s} = 13$ TeV after the LS1, ending in spring 2015.

References

- [1] CMS collaboration, JINST **3**, S08004 (2008).
- [2] CMS Collaboration, L1 and HLT approved trigger results (2012),
<https://twiki.cern.ch/twiki/bin/viewauth/CMSPublic/L1TriggerDPGResults>.
- [3] CMS Collaboration, PAS EWK-10-004 (2010), PAS LUM-12-001 (2012), PAS LUM-13-001 (2013).
- [4] CMS Collaboration, Luminosity - public results (2012),
<https://twiki.cern.ch/twiki/bin/view/CMSPublic/LumiPublicResults>.
- [5] CMS Collaboration, PAS FSQ-13-006 (2013).
- [6] R. J. Glauber and G. Matthiae, Nucl. Phys. **B** 21 (1970) 135.
- [7] COMPETE Collaboration, arXiv:hep-ph/0110170.
- [8] TOTEM Collaboration, JINST 3 (2008) S08007.
- [9] CMS Collaboration, PAS FSQ-12-026 (2012).
- [10] CMS Collaboration, PAS FSQ-12-031 (2012).
- [11] CMS Collaboration, PAS FSQ-12-035 (2012).
- [12] CMS Collaboration, PAS SMP-12-012 (2012).
- [13] CMS Collaboration, PAS SMP-12-028 (2012).
- [14] The Review of Particle Physics. J. Beringer et al. (Particle Data Group), Phys. Rev. D **86**, 010001 (2012).
- [15] H.-L. Lai et al., Phys. Rev. D **82** (2010) 074024, arXiv:1007.2241.
- [16] A. D. Martin, W. J. Stirling, R. S. Thorne, and G. Watt, Eur. Phys. J. C **63** (2009) 189, arXiv:0901.0002.
- [17] A. Martin, W. Stirling, R. Thorne, and G. Watt, Eur. Phys. J. C **64** (2009) 653, arXiv:0905.3531.
- [18] CMS Collaboration, PAS SMP-12-025 (2012).
- [19] T. Sjöstrand, S. Mrenna, P. Skands, JHEP **05** (2006) 026 (LU TP 06-13, FERMILAB-PUB-06-052-CD-T, hep-ph/0603175).
- [20] R. Gavin, Y. Li, F. Petriello, S. Quackenbush, Comput.Phys.Commun. **182** (2011) 2388-2403, ANL-HEP-PR-10-60, arXiv:1011.3540.
- [21] C. Oleari, Nucl.Phys.Proc.Suppl. **205-206** (2010) 36-41, arXiv:1007.3893.
- [22] J. Alwall, M. Herquet, F. Maltoni, O. Mattelaer, T. Stelzer, JHEP **1106** (2011) 128, FERMILAB-PUB-11-448-T, arXiv:1106.0522.
- [23] CMS Collaboration, CMS PAS-SMP-12-011, CERN-PH-EP-2013-217.
- [24] CMS Collaboration, CMS PAS-SMP-13-009.

- [25] S. Frixione and B.R. Webber, JHEP 0206 (2002) 029, arXiv:0204244.
- [26] U. Langenfeld, S. Moch, P. Uwer, Phys. Rev. **D** 80 (2009) 054009.
- [27] CMS Collaboration, CMS PAS-TOP-12-006.
- [28] CMS Collaboration, CMS PAS-TOP-12-007, CERN-PH-EP-2013-234.
- [29] CMS Collaboration, CMS PAS-TOP-11-021, CERN-PH-EP-2012-274.
- [30] CMS Collaboration, CMS PAS-SMP-11-018.

- [31] CMS Collaboration, JHEP12(2012) 035, CMS PAS-TOP-11-021, CERN-PH-EP-2012-274.

- [32] CMS Collaboration, CMS PAS-TOP-12-011.

- [33] CMS Collaboration, Phys. Rev. Lett. 110, 022003 (2013), CMS PAS-TOP-11-022.

- [34] CMS Collaboration, arXiv:1401.2942, CMS PAS-TOP-12-040, CERN-PH-EP-2013-237.

- [35] CMS Collaboration, CMS PAS-TOP-13-009.
- [36] L. Lyons, D. Gibaut, P. Clifford, Nucl. Instr. and Meth. A, 270 (1988) 110.

- [37] CMS Collaboration, CMS PAS-TOP-13-005.
- [38] L. Sonnenschein, Habilitation thesis,
http://www-d0.fnal.gov/results/publications_talks/thesis/sonnenschein/thesis.pdf,
Université Pierre et Marie Curie - Sorbonne Universités, Paris (2006).
- [39] CMS Collaboration, CMS PAS-HIG-13-015.
- [40] CMS Collaboration, CMS PAS-HIG-13-002.
- [41] CMS Collaboration, arXiv:1401.5041, CMS PAS-HIG-13-004, CERN-PH-EP-2014-001.
- [42] CMS Collaboration, CMS NOTE-2012-006.
- [43] CMS Collaboration, arXiv:1312.3310, CMS PAS-SUS-13-014.
- [44] CMS Collaboration, CMS PAS-SUS-13-011, CERN-PH-EP-2013-148.
- [45] CMS Collaboration, CMS PAS-SUS-12-024, CERN-PH-EP-2013-076.
- [46] CMS Collaboration, CMS PAS-SUS-13-007, CERN-PH-EP-2013-209.
- [47] CMS Collaboration, CMS PAS-SUS-13-013, CERN-PH-EP-2013-213.
- [48] CMS Collaboration, CMS PAS-SUS-13-008.
- [49] CMS Collaboration, CMS PAS-13-006.
- [50] CMS Collaboration, CMS PAS-13-017.
- [51] CMS Collaboration, CMS PAS-EXO-13-004.
- [52] CMS Collaboration, Phys. Lett. B 718 (2013) 795.
- [53] CMS Collaboration, arXiv:1305.0609, CERN-PH-EP/2013-077.